

# CrystEngComm

Accepted Manuscript



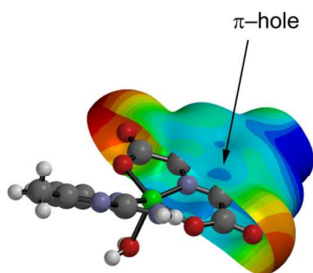
This is an *Accepted Manuscript*, which has been through the Royal Society of Chemistry peer review process and has been accepted for publication.

*Accepted Manuscripts* are published online shortly after acceptance, before technical editing, formatting and proof reading. Using this free service, authors can make their results available to the community, in citable form, before we publish the edited article. We will replace this *Accepted Manuscript* with the edited and formatted *Advance Article* as soon as it is available.

You can find more information about *Accepted Manuscripts* in the [Information for Authors](#).

Please note that technical editing may introduce minor changes to the text and/or graphics, which may alter content. The journal's standard [Terms & Conditions](#) and the [Ethical guidelines](#) still apply. In no event shall the Royal Society of Chemistry be held responsible for any errors or omissions in this *Accepted Manuscript* or any consequences arising from the use of any information it contains.

In this work, we synthesized and X-ray characterized four new complexes based on pyrazine- and pyridine-dicarboxylic acid ligands. In one compound, the formation of an unprecedented and counterintuitive  $lp-\pi$ -hole interaction involving the coordinated carboxylate group is noteworthy.



MEP (at  $\pi$ -hole) = 7.2 kcal/mol

## ARTICLE

# On the importance of non covalent interactions in the structure of coordination Cu(II) and Co(II) complexes of pyrazine- and pyridine-dicarboxylic acid derivatives: Experimental and theoretical views

Cite this: DOI: 10.1039/x0xx00000x

Received 00th January 2012,  
Accepted 00th January 2012

DOI: 10.1039/x0xx00000x

www.rsc.org/

Masoud Mirzaei<sup>a,\*</sup>, Hossein Eshtiagh-Hosseini<sup>a</sup>, Antonio Bauzá<sup>b</sup>, Sara Zarghami<sup>a</sup>, Pablo Ballester<sup>c</sup>, Joel T. Mague<sup>d</sup> and Antonio Frontera<sup>b,\*</sup>

Three Cu and one Co complexes of three pyridine-2,6-dicarboxylic acid derivatives were synthesized by proton transfer reactions. They are formulated as  $\{\text{Cu}[(\text{ampym})(\text{hypydc})(\text{H}_2\text{O})]\cdot\text{H}_2\text{O}$  (**1**),  $[\text{Co}(\text{pyzdc})(\text{H}_2\text{O})_2]\cdot\text{H}_2\text{O}$  (**2**),  $[\text{Cu}(\text{dipic})(\mu\text{-dipic})\text{Cu}(\text{II})(\text{H}_2\text{O})_5]\cdot 2\text{H}_2\text{O}$  (**3**) and  $[\text{Cu}_3(\text{dipic})_4(\text{en})_2]\cdot\text{en}\cdot 4\text{H}_2\text{O}$  (**4**) where *ampym* = 2-amino-4-methylpyrimidine, *hypydc* = 4-hydroxypyridine-2,6-dicarboxylic acid, *pyzdc* = pyrazine-2,3-dicarboxylic acid, *dipic* = pyridine-2,6-dicarboxylic acid, *en* = ethylenediamine. The complexes have been characterized by single crystal X-ray diffraction. Complex **1** is five-coordinated with a distorted square pyramidal geometry around Cu(II) where *hypydc* acts as a tridentate ligand, *ampym* as a monodentate ligand and one water molecule coordinated in the axial position. Complex **2** is a linear polymer containing six-coordinated Co(II) metal center, which is surrounded by N and O atoms from two *pyzdc* ligands and two coordinated water molecules. Complex **3** is a binuclear compound containing two six-coordinated Cu(II) ions, one coordinated to two *dipic* ligands while the other one is coordinated by five water molecules and one oxygen atom belonging to the bridging carboxylate group. Complex **4** is a trinuclear complex where two identical ions are hexa-coordinated to four carboxylate groups belonging to two *dipic* ligands and central ion is coordinated to two ethylenediamine ligands and two oxygen atoms of the *dipic* ligands. The non-covalent interactions that play important roles in the stabilization of the crystal structures have been analysed for several compounds by means of Density Functional Theory (DFT) calculations and characterized using the Bader's theory of "atoms in molecules" (AIM). The evaluation of the binding energies associated to each noncovalent interaction is useful for rationalizing their influence in the crystal packing. The formation of an unprecedented lp- $\pi$ -hole interaction in **1** is remarkable.

## Introduction

Nowadays the field of crystal engineering is a comprehensive discipline established by researchers with very different interests. Undoubtedly, the construction of fascinating topological architectures is one of the main attractions. Moreover, the modelling, synthesis, evaluation and utilization of crystalline solids having desired functions is also a main topic in crystal engineering.<sup>1,2</sup> Due to the delicate nature of competing weak forces the principle of designed synthesis of functional materials is very complicate, making difficult to succeed in a previously designed crystal engineering experiment.<sup>3</sup> The crystal structure prediction requires a precise understanding and a complete control over the intricate

interplay of weak noncovalent interactions responsible for crystal packing, since they are operating simultaneously.<sup>3-5</sup> To this respect, crystal engineering of nonlinear optical material is probably the most successful field. For instance, large macroscopic optical nonlinearities in ionic salt crystals has been developed.<sup>6</sup>

A great deal noncovalent forces are very frequently used by chemists to construct supramolecular assemblies, such as hydrogen-bonding,<sup>7</sup>  $\pi$ - $\pi$  stacking,<sup>8</sup> cation- $\pi$ <sup>9</sup> and C-H $\cdots$  $\pi$ <sup>10</sup> contacts. Moreover, lone pair (lp)- $\pi$ <sup>11</sup> and anion- $\pi$  interactions<sup>12</sup> have been increasingly reported in the literature. Moreover, the study of the impact of the acidity of reaction media leading to targeted species is still of transcendental

importance in crystal engineering including synthetic procedures at different pH levels that lead to different degree of protonation on the starting materials.<sup>13</sup> As a matter of fact, proton transfer is one of the most investigated chemical reactions in chemistry and biochemistry. It plays an important role in various chemical and biological processes such as stabilizing biomolecular structures, controlling the speed of enzymatic reactions as well as constructing supramolecular structures.<sup>14</sup> Recently, several types of forces such as coordination bonding, hydrogen bonding,  $\pi$ - $\pi$  stacking and electrostatic interactions<sup>7-11</sup> have been used in constructing extended supramolecular networks *via* proton transfer.<sup>15</sup> These reactions are caused by site-specific interaction such as hydrogen bonding.<sup>16</sup> The applications of H-bonding have been widely extended to various thermodynamic processes of industrial importance and fundamental research.<sup>17</sup> There are many interesting topological structures such as one-dimensional (1D) tapes, two-dimensional (2D) sheets, and three-dimensional (3D) networks which have been constructed through hydrogen bonding interactions. Among others, carboxylic acids have been successfully used in crystal engineering to generate a variety of 3D architectures (dimers, catemers, and bridged motifs).<sup>18</sup> Due to the above important applications of proton transfer compounds, our research group has been recently focused on preparing novel proton transfer compounds using various carboxylic acids.<sup>19</sup> In this report, four new complexes have been synthesized and their crystal structures determined. The solid state architecture of the complexes has been analysed and the noncovalent interactions have been energetically studied by means of DFT calculations. The evaluation of the binding energies associated to each noncovalent interaction is useful for rationalizing their influence in the crystal packing.

## Experimental Section

### General methods and materials

All reagents were purchased from commercial sources and used without further purification. The X-ray data were obtained with Bruker Smart-APEX and D8-Venture diffractometers.

**Synthesis of  $\{\text{Cu}(\text{ampym})(\text{hypyc})(\text{H}_2\text{O})\} \cdot \text{H}_2\text{O}$  (1).** An aqueous solution of copper(II) nitrate trihydrate (0.05 mmol) in distilled water (15 mL) was added to an aqueous solution of 4-hydroxypyridine-2,6-dicarboxylic acid (0.1 mmol) and 2-amino-4-methylpyrimidine (0.2 mmol) with stirring at 70–75°C for one hour. Suitable crystals were obtained by slow evaporation of the solvent at room temperature (Yield: 35%, m.p. > 300 °C). Elemental analysis: Anal. Calc. for  $\text{C}_{12}\text{H}_{14}\text{CuN}_4\text{O}_7$ : C, 36.94; H, 3.60; N, 14.36. Found: C, 36.88; H, 3.51; N, 14.30%. IR bands (KBr pellet,  $\text{cm}^{-1}$ ): 3375, 3190, 3115, 3065, 2963, 2853, 2722, 2618, 2516, 1624, 1590, 1482, 1375, 1296, 1168, 1115, 1045, 941, 868, 793, 746.

**Synthesis of  $\{\text{Co}(\text{pyzdc})(\text{H}_2\text{O})_2\} \cdot \text{H}_2\text{O}$  (2).** A aqueous solution (20 mL) of pyrazine-2,3-dicarboxylic acid (0.26 mmol) and 2-aminopyrazine (0.26 mmol) was stirred at 50–55°C for one hour. Then a solution of Co(II) nitrate

hexahydrate (0.15 mmol) was added and the reaction continued for two hours. Suitable crystals of **2** were obtained and collected after three months through a slow evaporation of the solvent at room temperature (Yield: 45%, m.p. > 300 °C). Elemental analysis: Anal. Calc. for  $\text{C}_6\text{H}_{10}\text{CoN}_2\text{O}_8$ : C, 24.23; H, 3.36; N, 9.42. Found: C, 24.18; H, 3.33; N, 9.40%. IR bands (KBr pellet,  $\text{cm}^{-1}$ ): 3375, 3200, 3115, 3062, 2960, 2853, 2720, 2615, 2516, 1624, 1595, 1482, 1377, 1296, 1170, 1120, 1045, 940, 865, 793, 745.

**Synthesis of  $[\text{Cu}(\text{dipic})(\mu\text{-dipic})\text{Cu}(\text{H}_2\text{O})_5] \cdot 2\text{H}_2\text{O}$  (3).** An aqueous solution of copper(II) nitrate trihydrate (0.05 mmol) in distilled water (15 mL) was added to an aqueous solution of pyridine-2,6-dicarboxylic acid (0.1 mmol) and 2-amino-4-methylpyrimidine (0.2 mmol) with stirring at 70–75°C for one hour. Suitable crystals were obtained by slow evaporation of the solvent at room temperature (Yield: 40%, m.p. > 300 °C). Elemental analysis: Anal. Calc. for  $\text{C}_{14}\text{H}_{20}\text{Cu}_2\text{N}_2\text{O}_{15}$ : C, 28.80; H, 3.42; N, 4.80. Found: C, 28.68; H, 3.35; N, 4.75%. IR bands (KBr pellet,  $\text{cm}^{-1}$ ): 3370, 3190, 3120, 3062, 2962, 2850, 2720, 2616, 2516, 1625, 1595, 1480, 1377, 1295, 1168, 1116, 1045, 941, 865, 795, 747.

**Synthesis of  $[\text{Cu}_3(\text{dipic})_4(\text{en})_2] \cdot \text{enH}_2 \cdot 4\text{H}_2\text{O}$  (4).** To a boiling solution of distilled water (25 mL) and four drops of *en* (0.2 mL) containing 1 mmol *dipic* acid was added copper(II) acetate monohydrate (1 mmol) and a lesser extent of  $\text{NH}_4\text{PF}_6$ . The resulting solution was stirred at 100 °C for 3 hours. Dark blue crystals were obtained after a week by slow evaporation of solvent (Yield: 35%, m.p. > 300 °C). Elemental analysis: Anal. Calc. for  $\text{C}_{34}\text{H}_{46}\text{Cu}_3\text{N}_{10}\text{O}_{20}$ : C, 36.91; H, 4.16; N, 12.66. Found: C, 36.88; H, 4.10; N, 12.60%. IR bands (KBr pellet,  $\text{cm}^{-1}$ ): 3375, 3190, 3114, 3062, 2964, 2853, 2725, 2616, 2520, 1624, 1591, 1485, 1377, 1295, 1170, 1116, 1045, 940, 865, 793, 750.

### Crystallography

A thick blue-green plate-like crystal of **1** and an orange block-like crystal of **2** were mounted on Mitegen loops with a drop of Paratone oil and placed in a cold nitrogen stream on the diffractometer. The diffraction data for **1** were obtained on the Smart APEX from 3 sets of 400 frames, each of width 0.5° in  $\omega$ , collected at  $\varphi = 0.0, 90.00$  and  $180.00^\circ$  and 2 sets of 800 frames, each of width 0.45° in  $\varphi$ , collected at  $\omega = -30.00$  and  $210.00^\circ$ . The scan time was 20 sec/frame. The diffraction data for **2** were obtained on the D8-Venture from 8 sets of 340 frames, each of width 0.5° in  $\omega$ , collected at  $\varphi = 0.00, 90.00, 180.00$  and  $270.00^\circ$  and at  $2\theta = -50.00$  and  $-90.00^\circ$  and 4 sets of 340 frames, each of width 0.5° in  $\omega$  collected at  $2\theta = -90.00^\circ$  and  $\varphi = 45.00, 135.00, 225.00$  and  $315.00^\circ$ . The scan time was 15 sec/frame. In both cases the intensity data were collected under the control of the APEX20 software and the raw data integrated and corrected for Lorentz and polarization effects with SAINT.<sup>21</sup> Empirical absorption corrections and averaging of equivalent reflections were carried out with SADABS.<sup>22</sup> The structures were solved by direct methods (SHELXS<sup>23</sup>) and refined by full-matrix, least-squares methods (SHELXL<sup>23</sup>). Crystallographic data for **3** was collected at 100(2) K on a Bruker Kappa APEX II DUO diffractometer equipped with an

APPEX 2 4K CCD area detector and a microsource with MoK $\alpha$  radiation ( $\lambda = 0.71073 \text{ \AA}$ ). The raw frame data were processed using SAINT and SADABS to yield the reflection data file.<sup>21,22</sup> The structures were solved by Direct Methods using SIR2011<sup>24</sup> and refined on  $F^2$  by full-matrix least-squares procedures, using SHELXL-97.<sup>23</sup> Crystal data collection and refinement details are given in Table 1.

### Theoretical methods

The geometries of the complexes included in this study were computed at the BP86-D3/def2-TZVPD level of theory using the crystallographic coordinates within the TURBOMOLE program.<sup>25</sup> The basis set superposition error for the calculation of interaction energies has been corrected using the counterpoise method.<sup>26</sup> The “atoms-in-molecules” (AIM)<sup>27</sup> analysis of the electron density has been performed at the same level of theory using the AIMAll program<sup>28</sup> and the geometry obtained from the crystallographic coordinates.

### Results and discussion

#### Crystal structure of 1

The structure of **1** is shown in Fig. 1 (left) and selected bond lengths and angles are summarized in Table 2. The asymmetric unit consists of a neutral Cu(II) complex ligated by one hypydc unit, one 2-amino-4-methylpyrimidine and one water molecule together with one uncoordinated water molecule.

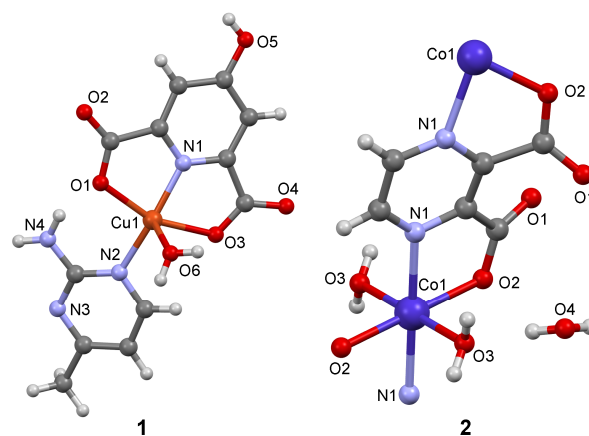


Fig. 1 Molecular structure of complexes **1** and **2** with indication of the atom numbering scheme.

Table 2 Selected bond lengths ( $\text{\AA}$ ) and angles ( $^\circ$ ) for compound **1**

O1–Cu1	2.013(1)	O1–Cu1–N1	81.06(5)
O3–Cu1	2.071(1)	O3–Cu1–N1	78.81(5)
O6–Cu1	2.230(2)	O6–Cu1–N1	99.94(6)
N1–Cu1	1.906(1)	N2–Cu1–N1	163.75(6)
N2–Cu1	1.974(1)	O1–Cu1–N2	100.64(6)
O3–Cu1–O1	159.31(5)	O3–Cu1–N2	97.36(5)
O6–Cu1–O1	95.79(6)	O6–Cu1–N2	95.97(6)
O6–Cu1–O3	92.38(6)		

The coordination geometry of the Cu atom can be described as

Table 1. Crystal data structure for compounds **1–4**.

	<b>1</b>	<b>2</b>	<b>3</b>	<b>4</b>
Empirical formula	C <sub>12</sub> H <sub>14</sub> CuN <sub>4</sub> O <sub>7</sub>	C <sub>6</sub> H <sub>10</sub> CoN <sub>2</sub> O <sub>8</sub>	C <sub>14</sub> H <sub>20</sub> Cu <sub>2</sub> N <sub>2</sub> O <sub>15</sub>	C <sub>34</sub> H <sub>46</sub> Cu <sub>3</sub> N <sub>10</sub> O <sub>20</sub>
Formula weight	389.81	297.09	583.42	1105.43
Temperature/K	150(2)	100(2)	100(2)	293(2)
Crystal system	monoclinic	monoclinic	monoclinic	monoclinic
Space group	P2 <sub>1</sub> /c	C2/c	P2 <sub>1</sub> /c	P2 <sub>1</sub> /n
a/ $\text{\AA}$	11.986(2)	12.5445(4)	8.3425(5)	8.152(2)
b/ $\text{\AA}$	7.660(1)	7.3874(3)	27.164(2)	20.538(5)
c/ $\text{\AA}$	15.750(3)	11.8763(6)	9.5946(6)	12.736(3)
$\alpha/^\circ$	90	90	90	90
$\beta/^\circ$	94.123(3)	111.118(1)	98.111(2)	93.44(2)
$\gamma/^\circ$	90	90	90	90
Volume/ $\text{\AA}^3$	1442.3(5)	1026.68(7)	2152.5(2)	2128.5(10)
Z	4	4	4	2
$\rho_{\text{calc}}/\text{mg}/\text{mm}^3$	1.795	1.922	1.800	1.725
$\mu/\text{mm}^{-1}$	1.562	13.529	2.055	1.579
F(000)	796.0	604.0	1184.0	1134.0
Crystal size/ $\text{mm}^3$	0.16 × 0.12 × 0.08	0.16 × 0.14 × 0.08	0.30 × 0.30 × 0.30	0.51 × 0.28 × 0.12
2 $\theta$ range for data collection	5.18 to 58.24 $^\circ$	14.18 to 139.34 $^\circ$	2.62 to 39.61	5.38 to 70.34 $^\circ$
Index ranges	–16 ≤ h ≤ 16 –10 ≤ k ≤ 10 –21 ≤ l ≤ 21	–15 ≤ h ≤ 15 –8 ≤ k ≤ 8 –14 ≤ l ≤ 14	–14 ≤ h ≤ 14 –48 ≤ k ≤ 48 –17 ≤ l ≤ 17	–13 ≤ h ≤ 13 –33 ≤ k ≤ 33 –20 ≤ l ≤ 20
Reflections collected	25054	8419	55047	35349
Independent reflections	3804 [R(int) = 0.0567]	951 [R(int) = 0.0312]	12365 [R(int) = 0.0205]	9453 [R(int) = 0.0339]
Data/restraints/parameters	3804/0/218	951/0/80	12365/14/341	9453/5/336
Goodness-of-fit on $F^2$	1.047	1.091	1.171	1.019
Final R indexes [ $I > 2\sigma(I)$ ]	R <sub>1</sub> = 0.0305, wR <sub>2</sub> = 0.0810	R <sub>1</sub> = 0.0198, wR <sub>2</sub> = 0.0548	R <sub>1</sub> = 0.0400, wR <sub>2</sub> = 0.1253	R <sub>1</sub> = 0.0351, wR <sub>2</sub> = 0.0903
Final R indexes [all data]	R <sub>1</sub> = 0.0352, wR <sub>2</sub> = 0.0847	R <sub>1</sub> = 0.0201, wR <sub>2</sub> = 0.0551	R <sub>1</sub> = 0.0426, wR <sub>2</sub> = 0.1237	R <sub>1</sub> = 0.0594, wR <sub>2</sub> = 0.1002
Largest diff. peak/hole / e $\text{\AA}^{-3}$	0.59/–0.40	0.34/–0.28	–	0.48/–0.47

distorted square pyramid with the basal plane defined by one N atom and two O atoms from the deprotonated 4-hydroxypyridine-2,6-dicarboxylate ligand and one ring N atom from the 2-amino-4-methylpyrimidine ligand and a water molecule in the apical position. Selected bond length and angles are summarized in Table 2. Intra ligand bond lengths and angles are in the range expected for these coordinated ligands. As we expected the axial bond (2.22 Å) is longer than the others and it can be attributed to Jahn–Teller effect. It should be noted that the Cu1–N2 bond (1.974(1) Å) is longer than the Cu1–N1 bond (1.906(1) Å) which is likely due to the geometrical constraints of the *hypydc* ligand. The packing diagram of **1** is shown in the supplementary material (see Fig. S1). Adjacent complexes are connected *via* various non-covalent interactions to generate a two-dimensional supramolecular structure. Different hydrogen bonds such as N4–H4A···O7, O6–H6A···O4 and O7–H7B···O2 have a crucial role in creating this 2D network (see Fig. 2 and Table 3).

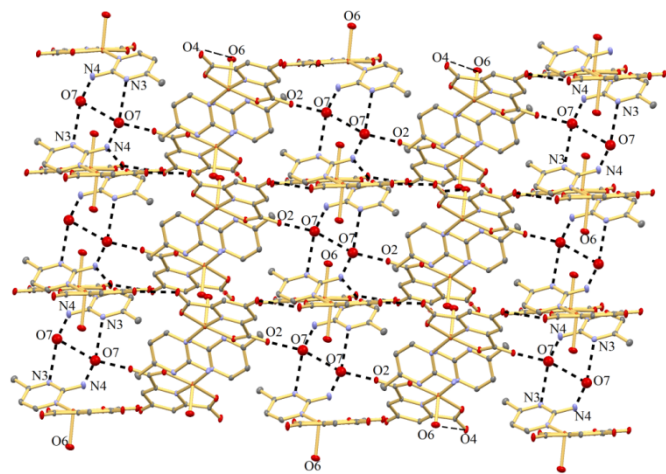


Fig. 2 Various N–H···O and O–H···O H-bonding forming 2–D network of **1**.

Table 3 Hydrogen bonding parameters of **1**

D	H	A	d(D–H)/Å	d(H–A)/Å	d(D–A)/Å	D–H–A/°
O5	H5O	O4 <sup>1</sup>	0.84	1.86	2.684(2)	167
O6	H6A	O4 <sup>2</sup>	0.84	2.14	2.974(2)	173
O6	H6B	O7 <sup>3</sup>	0.84	1.99	2.831(2)	176
N4	H4A	O7 <sup>4</sup>	0.91	2.04	2.951(2)	174
N4	H4B	O1	0.91	1.94	2.808(2)	158
O7	H7A	N3 <sup>5</sup>	0.84	2.07	2.881(2)	161
O7	H7B	O2 <sup>1</sup>	0.84	1.89	2.713(2)	165

<sup>1</sup>+X,3/2–Y,1/2+Z; <sup>2</sup>–X,2–Y,–Z; <sup>3</sup>+X,+Y,–1+Z; <sup>4</sup>1–X,1–Y,1–Z; <sup>5</sup>+X,1+Y,1+Z

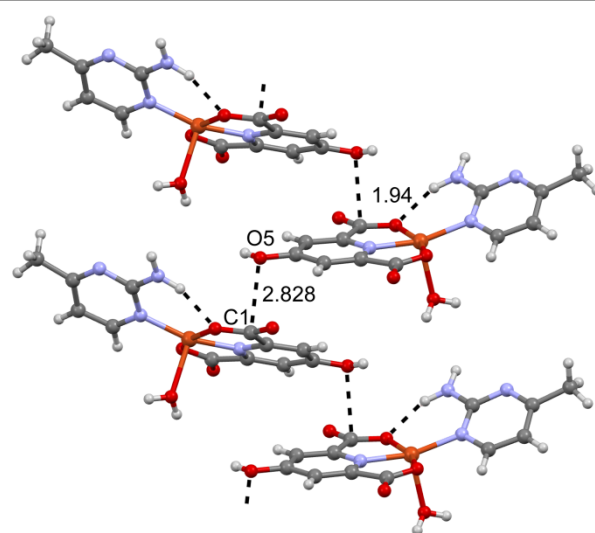


Fig. 3 Partial view of the crystal packing of **1** with indication of the lp– $\pi$ -hole interaction. Distances in Å.

The solid state packing of compound **1** presents a very relevant noncovalent interaction that is formed between the lone pair of the hydroxylic oxygen atom (O5) and the carbon atom (C1) of the carboxylate group (see Fig. 3). This can be classified as a  $\pi$ -hole interaction, where the electron donor is the oxygen atom and the acceptor is the carbon atom belonging to carboxylate group that is coordinated to the Cu<sup>II</sup> metal center and consequently most of the negative electron charge is transferred to the metal cation. In addition, this carboxylate group also participates in a strong intramolecular bond with the NH<sub>2</sub> group of the coligand, which further contributes to the  $\pi$ -acidity of the carbon atom. The distance is very short (2.828 Å) indicating a strong interaction. To the best of our knowledge this  $\pi$ -hole interaction (between a coordinated carboxylate and a lone pair, see ESI) has not been previously described in the literature. Theoretically, a related interaction between the NH<sub>3</sub> electron donor and the  $\pi$ -hole of X–NO<sub>2</sub> molecules has been previously reported.<sup>29</sup> This lp– $\pi$ -hole interaction between the O5 and the C1 will be further analyzed energetically in the theoretical study (*vide infra*). We have search the Cambridge Structural Database to investigate if this interaction is frequent in crystal structures similar to compound **1**. As a result, we have found only 6 structures exhibiting lp– $\pi$ -hole interactions between hydroxylic oxygen atoms and carboxylate groups coordinated to Cu(II). Interestingly, the number of hits is greater (58) if the molecule that acts as Lewis base is water. The reference codes of both searches are included in the ESI (see Table S1) and two selected examples are also represented.

## 5.2 Crystal structure of **2**

A perspective view of the repeat unit of the chain with the atom numbering scheme of compound **2** is shown in Fig. 1 (right) while the packing diagram is shown in the ESI (Fig. S2). Selected bond lengths and angles are shown in Table 4. In compound **2** the *pyzdc* ligand is coordinated to the cobalt ion as a bis(bidentate) bridging ligand with each cobalt ion

coordinated by two nitrogen atoms and four oxygen atoms from two different *pyzdc* ligands. Two water molecules are also coordinated to the metal ion in a *trans* arrangement leading to a distorted octahedral geometry. The Co atom lies on a crystallographic center of symmetry while a crystallographic two-fold axis bisects the C–C bonds of the pyrazine ring. With the dianionic *pyzdc* ligands bridging the cobalt ions, extended linear 1–D chains are formed along the *b* axis (Fig. 4). Thus the complex exhibits one-dimensional coordination polymeric structures made by linear arrays of Co(II) metal ions.

**Table 4** Selected bond lengths (Å) and angles (°) for compound **2**

Co1–O2	2.061(1)	O3 <sup>1</sup> –Co1–O3	180.00(7)
Co1–O3	2.098(1)	N1 <sup>1</sup> –Co1–O3 <sup>1</sup>	88.27(4)
N1–Co1	2.128(1)	N1 <sup>1</sup> –Co1–O3	91.73(4)
N1 <sup>1</sup> –Co1–O2	101.44(5)	N1 <sup>1</sup> –Co1–O2	101.44(5)
N1–Co1–O2	78.56(5)		

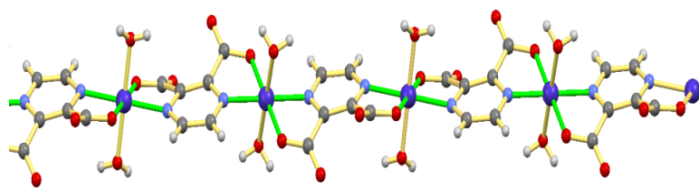


**Fig. 4** Perspective view of the one-dimensional polymeric structure of **2** along the *b* axis. Color code: Co in dark blue, N in light blue, O in red and C in grey.

These chains are linked together by strong O—H···O interactions such as O(3)—H···O(1), O(3)—H···O(4) and O(4)—H···O(2) (see Table 5). These non-covalent interactions help to build up a three-dimensional network and increase the stability of the supramolecular structure (Fig. 5).

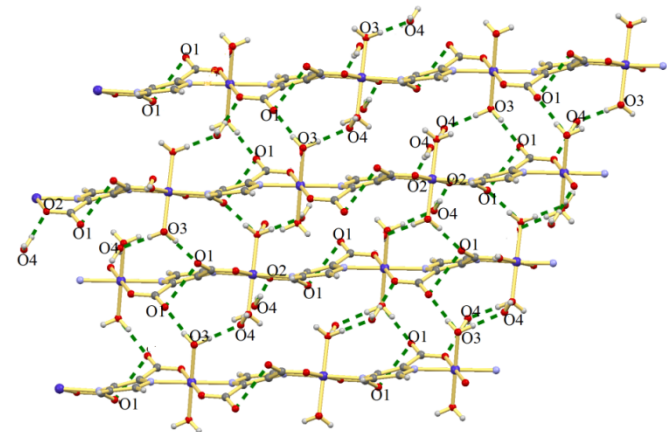


**Fig. 5** 1–D linear chains link together by O–H···O hydrogen bonds to form a 3–D network.

**Table 5** Hydrogen bonding parameters of **2**

D	H	A	d(D–H)/Å	d(H–A)/Å	d(D–A)/Å	D–H–A/°
O3	H3A	O11	0.85	1.87	2.711(2)	173
O3	H3B	O42	0.85	1.80	2.650(2)	179
H4	H4A	O23	0.85	1.99	2.835(2)	170
O4	H4B	O34	0.85	2.26	3.057(2)	156

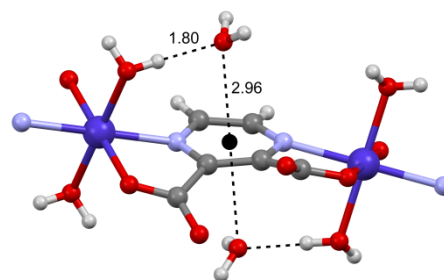


**Fig. 6** Partial view of the crystal packing of **2** with indication of the lp– $\pi^*$ –lp assembly and H–bonding interactions. Distances in Å.

It is worth mentioning the position of the uncoordinated water molecules in the solid state structure. The water oxygen atoms of the water molecules are very close to the aromatic center of the pyrazine ring (2.96 Å) at opposite sides of the ring forming an “inverse sandwich” (lp– $\pi^*$ –lp assembly, see Fig. 6). The  $\pi$ -acidity of the pyrazine ring is enhanced by the coordination of the aromatic nitrogen atoms to the Co<sup>II</sup> metal ions. We have denoted the interaction as lp– $\pi^*$ , to illustrate that the aromatic ring is electron deficient and consequently adequate for interacting lp donor molecules. The other lone pair of the oxygen atom of the water molecule is pointing to one coordinated water molecule and thus it is simultaneously forming a strong hydrogen bond (1.80 Å). The acidity of the hydrogen atom of the water molecule is enhanced due to its coordination to the metal. This interesting combination of hydrogen bonding interactions and lp– $\pi^*$ –lp assembly is responsible for the final location of the non coordinated water molecules. The relative strength of the aforementioned noncovalent interactions is further discussed below.

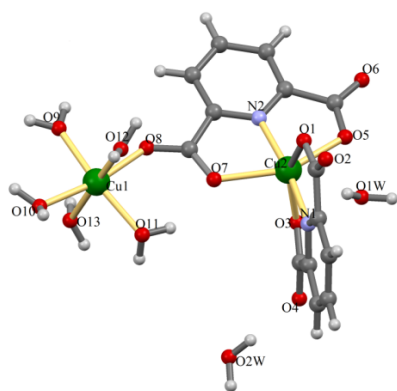
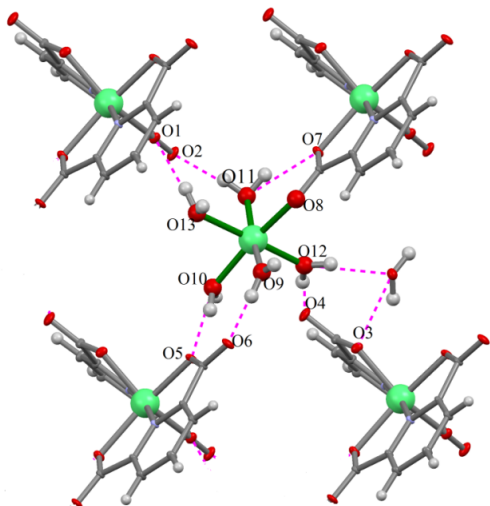
### 5.3 Crystal structure of **3**

The coordination environment of copper(II) ions is shown in Fig. 7. Selected bond lengths and angles of the metal coordination sphere are shown in Table 6. Moreover, a view of the packing is depicted in the ESI (Fig. S3).

The two *dipic* ligands are deprotonated in the complex as both are coordinated in a tridentate manner to one copper atom. One of the two *dipic*<sup>2–</sup> groups also acts as a bridging ligand to the pentaqua–Cu(II) unit. Both Cu(II) ions exhibit distorted octahedral geometry with Cu(1) coordinated by six oxygen atoms, five from coordinated water molecules and one from a carboxyl group of *dipic*<sup>2–</sup> of which the other oxygen atom is linked to Cu(2). Cu(2) is coordinated by four oxygen atoms of four carboxyl groups and two nitrogen atoms which are all from *dipic*<sup>2–</sup> ligand. Cu–O bond lengths are at the range expected, however it should be noted that coordination of O(8) atom to Cu(1) results in a slight lengthening of the Cu(2)–O(7) bond (2.213(1) Å) as compared with the three others (Cu(2)–O(1) = 2.170(1) Å, Cu(2)–O(3) = 2.113(1) Å, Cu(2)–O(5) = 2.178(1) Å) (Table 2). Hydrogen bonds between coordinated water molecules and the carboxylate oxygen atoms of the *dipic*<sup>2–</sup> ligands link the binuclear copper molecules to form a one-dimensional chain (Fig 8).

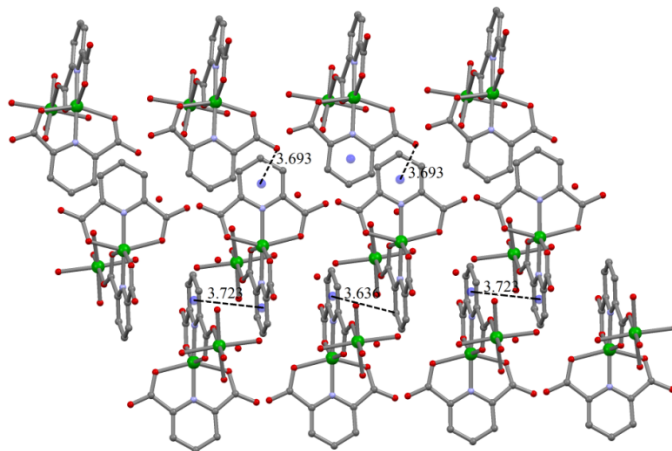
**Table 6** Selected bond lengths (Å) and angles (°) for **3**

Cu1–O12	2.053(1)	O8–Cu1–O10	170.39(4)
Cu1–O9	2.057(1)	O12–Cu1–O13	176.53(5)
Cu1–O11	2.085(1)	O9–Cu1–O13	86.02(5)
Cu1–O8	2.088(1)	O11–Cu1–O13	89.38(4)
Cu1–O10	2.090(1)	O8–Cu1–O13	95.36(4)
Cu1–O13	2.165(1)	O10–Cu1–O13	85.79(4)
Cu2–N1	2.021(1)	N1–Cu2–N2	171.79(4)
Cu2–N2	2.027(1)	N1–Cu2–O3	76.61(4)
Cu2–O3	2.113(1)	N2–Cu2–O3	104.94(4)
Cu2–O1	2.170(1)	N1–Cu2–O1	75.73(4)
Cu2–O5	2.178(1)	N2–Cu2–O1	104.13(4)
Cu2–O7	2.213(1)	O3–Cu2–O1	149.91(4)
O12–Cu1–O9	96.67(6)	N1–Cu2–O5	112.54(4)
O12–Cu1–O11	88.37(5)	N2–Cu2–O5	75.67(4)
O9–Cu1–O11	168.54(5)	O3–Cu2–O5	85.16(4)
O12–Cu1–O8	87.30(5)	O1–Cu2–O5	94.64(4)
O9–Cu1–O8	79.72(4)	N1–Cu2–O7	95.59(4)
O11–Cu1–O8	90.28(4)	N2–Cu2–O7	76.24(4)
O12–Cu1–O10	91.97(5)	O3–Cu2–O7	97.58(5)
O9–Cu1–O10	90.85(4)	O1–Cu2–O7	96.68(4)
O11–Cu1–O10	99.29(4)	O5–Cu2–O7	151.51(4)

**Fig. 7** Molecular structure of **3** with indication of the atom numbering scheme.**Fig. 8.** O–H...O hydrogen bonds (pink-dashed lines) link the binuclear copper molecules in **3** to form a one-dimensional chain.

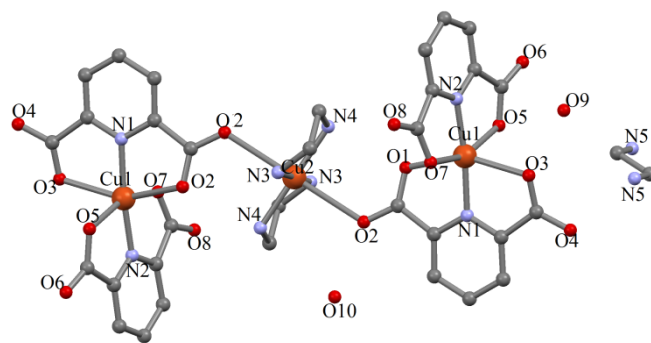
As can be seen in Fig. 9, the final 3D architecture is dominated by aromatic interactions involving the pyridine-2,6-

dicarboxylic acid ligands such as  $\pi$ - $\pi$  (3.72 Å) and CO- $\pi^*$  (3.693 Å) in addition to the hydrogen bonding network described above. These noncovalent interactions are further studied below in the theoretical analysis of the interactions.

**Fig. 9** Representation of  $\pi$ - $\pi$ , CO- $\pi^*$  and C-H... $\pi$  interactions between pyridine-2,6-dicarboxylic acid ligands which generates a three-dimensional network in **3**.

#### 5.4 Crystal structure of **4**

Compound **4** crystallizes in the monoclinic  $P2_1/n$  space group and its molecular structure including the atom labelling scheme is given in Fig 10. The crystal data collection is summarized in Table 1 and selected bond length and angles are gathered in Table 7.

**Fig. 10** Molecular structure of **4** with indication of the atom numbering scheme.**Table 7** Selected bond lengths (Å) and angles (°) for **4**

N1–Cu1	1.9549(11)	O7–Cu1–N1	95.33(4)
O5–Cu1	2.1328(11)	O3–Cu1–O5	84.60(5)
O3–Cu1	1.9228(11)	O1–Cu1–O5	97.89(5)
N2–Cu1	2.2808(11)	N1–Cu1–N2	173.52(4)
O1–Cu1	2.1030(11)	O5–Cu1–N2	78.49(4)
O7–Cu1	2.0080(13)	O1–Cu1–O7	88.96(5)
N4–Cu2	2.0080(13)	N4–Cu2–N4 <sup>1</sup>	180.00(6)
N4 <sup>1</sup> –Cu2	2.0019(16)	N4–Cu2–N3	83.80(6)
O5–Cu1–N1	107.04(4)	N4–Cu2–N3 <sup>1</sup>	96.20(6)
O3–Cu1–N1	76.64(4)	N4 <sup>1</sup> –Cu2–N3 <sup>1</sup>	83.80(6)
O1–Cu1–N1	76.64(4)	N4 <sup>1</sup> –Cu2–N3	96.20(6)

The molecular structure diagram shows that this compound is a trinuclear complex with two different types of metal centers,

Cu1 and Cu2 metal ions (see Fig. 10). Both Cu1 atoms are hexa-coordinated to four oxygen and two nitrogen atoms of two pyridine-2,6-dicarboxylic acid ligands (*dipic*). The aromatic rings are almost perpendicular to each other resulting in a distorted octahedral coordination sphere around Cu1. The coordination number for Cu2 is also six since it is coordinated to two ethylenediamine groups and two oxygen atoms of *dipic* ligands. Therefore, the structure can be defined as two Cu1 complexes that are acting as monodentate ligands for Cu2 in axial positions. Moreover, there are two uncoordinated water and one diprotonated ethylenediamine molecules in the repeat unit that act as counterions. The packing diagram of the structure is shown in Fig. S5. As can be seen in Fig. 11, N-H...O hydrogen bonds between ethylenediamine moieties and water molecules form six-membered rings that generate infinite 1D ribbons. These ribbons interact at both sides with the trinuclear complexes generating a 2D supramolecular plane by means of additional hydrogen bonds (N-H...O=C) with the carboxylate groups. Furthermore,  $\pi$ - $\pi$  interactions with inter-centroid distance of 3.507 Å between the pyridine rings are crucial for the formation of the final 3D architecture, as can be observed in Fig. 12. Interestingly, each trinuclear complex establishes four equivalent stacking interactions with four neighbouring complexes using the pyridine rings.

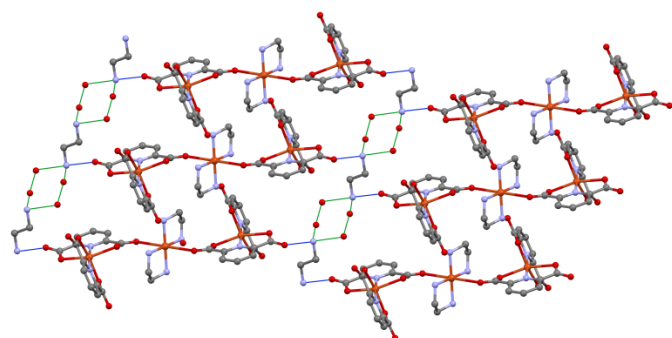


**Fig. 11.** 2D layer observed in **4**. Hydrogen bonding interactions involving water molecules are represented in green. N-H...O=C hydrogen bonds are represented in blue. Hydrogen atoms are omitted for clarity.

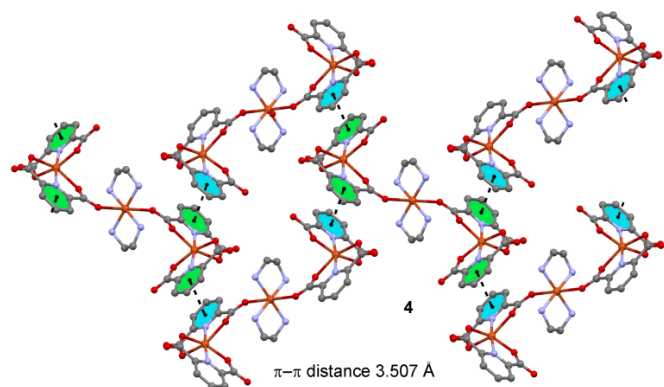


**Fig. 12.** Representation of  $\pi$ - $\pi$  interactions observed in **4**. Hydrogen atoms are omitted for clarity.

### Theoretical study

In this part of the manuscript we analyze the interesting and uncommon noncovalent interactions and assemblies observed in the solid state architectures of the Cu<sup>II</sup> and Co<sup>II</sup> coordination complexes. We have started by studying the  $\pi$ -hole interaction described above for compound **1**, where an lp of the phenolic oxygen atom is pointing to the carbon atom of the coordinated carboxylate group. In Fig. 13 we show the interaction energy of the dimer and the molecular electrostatic potential surface of one monomer. The  $\pi$ -hole is clearly observed in the MEP surface (see Fig. 13, right) and the oxygen atom in the solid state structure is exactly located in the  $\pi$ -hole, in agreement with the theoretical analysis. The interaction energy computed for this interaction is -4.2 kcal/mol, which is similar to lp- $\pi$  interactions previously reported involving aromatic rings.<sup>13</sup>

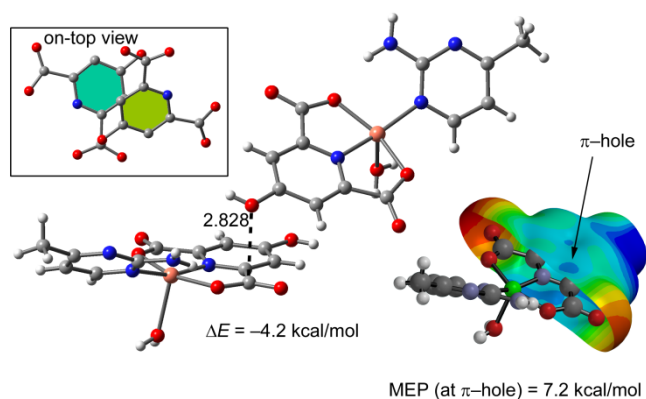


**Fig. 13** Left: Partial view of the X-ray crystal packing of **1** with indication of the  $\pi$ -hole interaction and the associated binding energy. In the on-top view (top-left) the hydrogen atoms, Cu ions and the coligands have been omitted for clarity. Right: Molecular electrostatic potential surface computed for **1**.

Due to the polymeric nature of **2**, we have used a theoretical model that includes two Co ions and three pyrazine ligands in order to reduce the size of the system for computational purposes. We have analyzed energetically the double lp- $\pi^*$  interaction observed in the solid state between the water molecules and the pyrazine ring. We have also analyzed the relative importance of this interaction with respect to the hydrogen bond that the same water molecule is establishing with the Co-coordinated water molecule. Finally we have also studied the influence of the coordination of Co on the strength of the lp- $\pi^*$  interaction. In Fig. 14 we represent the theoretical models and the interaction energies and it can be observed that the interaction energy computed for the dimer where two H-bonds and two lp- $\pi$  interactions are established (left) is large and negative,  $\Delta E(\text{HB} + \text{lp}-\pi^*) = -16.7$  kcal/mol. When the coordinated water molecules that form the H-bonding interactions are eliminated from the theoretical model the interaction energy is significantly reduced to  $\Delta E(\text{lp}-\pi^*) = -7.9$  kcal/mol. Therefore each H-bonding interaction is approximately -4.4 kcal/mol and each lp- $\pi$  interaction contributes in -3.95 kcal/mol. Finally, if the transition metals and other ligands are eliminated from the theoretical model, the

interaction energy is further reduced to  $\Delta E^*(lp-\pi^*) = -3.2$  kcal/mol, which indicated that each  $lp-\pi^*$  interaction without the electron withdrawing effect of the transition metal would be reduced to  $-1.6$  kcal/mol. In the latter theoretical model (see Fig. 14, right), the carboxylate groups have been protonated in order to preserve the charge of the system neutral.

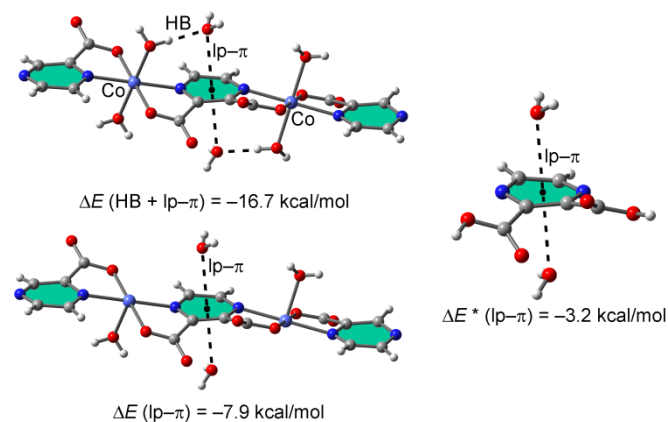


Fig. 14 Theoretical models and interaction energies computed for **2**.

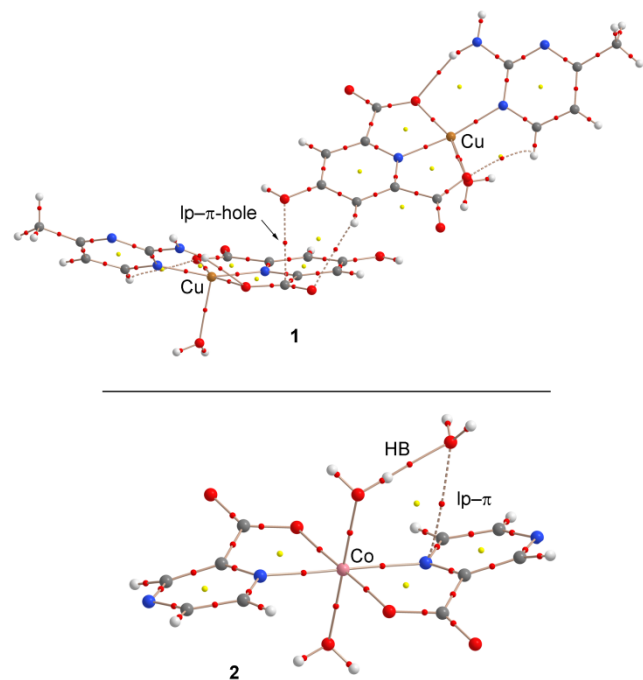


Fig. 15 Distribution of bond (red) and ring (yellow) critical points obtained for the theoretical models of **1** (left) and **2** (right). The solid bond paths represent covalent bonds and dashed bond paths represent noncovalent bonds.

We have also computed the distribution of critical points for the dimer observed in **1** in order to confirm the existence of the  $lp-\pi$ -hole interaction and in **2** to characterize the H-bonding and  $lp-\pi^*$  interaction using the Bader's theory of atoms in molecules that provides an unambiguous definition of chemical bonding. The representations of critical points and bond paths are shown in Fig. 15. It can be clearly observed a bond critical

point ( $\rho(r) = 1.131 \times 10^{-2}$  a.u.) connecting the hydroxyl oxygen atom with the carbon atom of the carboxylate group in the dimer of **1**. In **2**, the hydrogen bond is characterized by the presence of a bond critical point connecting both coordinated and non coordinated water molecules and the  $lp-\pi^*$  interaction is characterized by the presence of bond critical point ( $\rho(r) = 0.772 \times 10^{-2}$  a.u.) connecting the oxygen atom of the non coordinated water molecule with the aromatic nitrogen atom. The distribution of critical points shown in Fig. 15 further confirms the existence of both  $lp-\pi$ -hole and  $lp-\pi^*$  interaction in the solid state of **1** and **2**, respectively. The value of the Laplacian of the electron density computed at the aforementioned bond critical points are positive, as is common in closed shell interactions. In addition, the value of the charge density  $\rho(r)$  at the bond critical points is in the range of previously described for these<sup>30</sup> and other types<sup>31</sup> of weak interactions.

For **3**, we have focused our attention to the analysis of both  $\pi-\pi$  and  $lp-\pi^*$  interactions that are crucial determining the crystal packing, as previously described and discussed (see Fig. 8). Mainly, we have studied the influence of the coordination of the ligand to the transition metal in the strength of both interactions. The theoretical models used and the interaction energies are shown in Fig. 16 for both complexes. In the top part of Fig. 16 we show the results for the  $\pi-\pi$  interaction and dimer observed in the solid state has very large and negative interaction energy [ $\Delta E(\text{HB} + \pi-\pi) = -67.2$  kcal/mol] because, in addition to the  $\pi-\pi$  stacking interaction, two strong hydrogen bonds are simultaneously formed. We have used a theoretical model where the coordinated water molecules have been eliminated and consequently the hydrogen bonds cannot be formed. The interaction energy of this model is reduced to  $\Delta E(\pi-\pi) = -42.1$  kcal/mol, indicating that each hydrogen bond has an associated binding energy of  $-7.5$  kcal/mol. We have also computed the interaction energy of the stacking without the presence of the transition metals and the interaction energy is further reduced to  $\Delta E^*(\pi-\pi) = -10.7$  kcal/mol, therefore the coordination of the aromatic ligand to the Cu metal centers has a strong influence on the interaction energy. In this model the carboxylate groups have been protonated to keep the charge of the system neutral.

The  $lp-\pi^*$  interaction has been also analyzed and the results are shown in the bottom part of Fig. 16. The interaction energy computed for this interaction,  $\Delta E(lp-\pi^*) = -21.6$  kcal/mol, is considerably smaller (in absolute value) than the one computed for the  $\pi-\pi$  interaction. For this interaction the effect of the coordination of the metal to the interaction energy is also very important, since in the absence of the Cu(II) ions the interaction energy is reduced to  $\Delta E^*(lp-\pi^*) = -5.5$  kcal/mol.

## Conclusions

In this work, we synthesized and X-ray characterized four new complexes based on pyrazine- and pyridine-dicarboxylic acid ligands. In compound **1**, the formation of an unprecedented and counterintuitive  $lp-\pi$ -hole interaction involving the coordinated

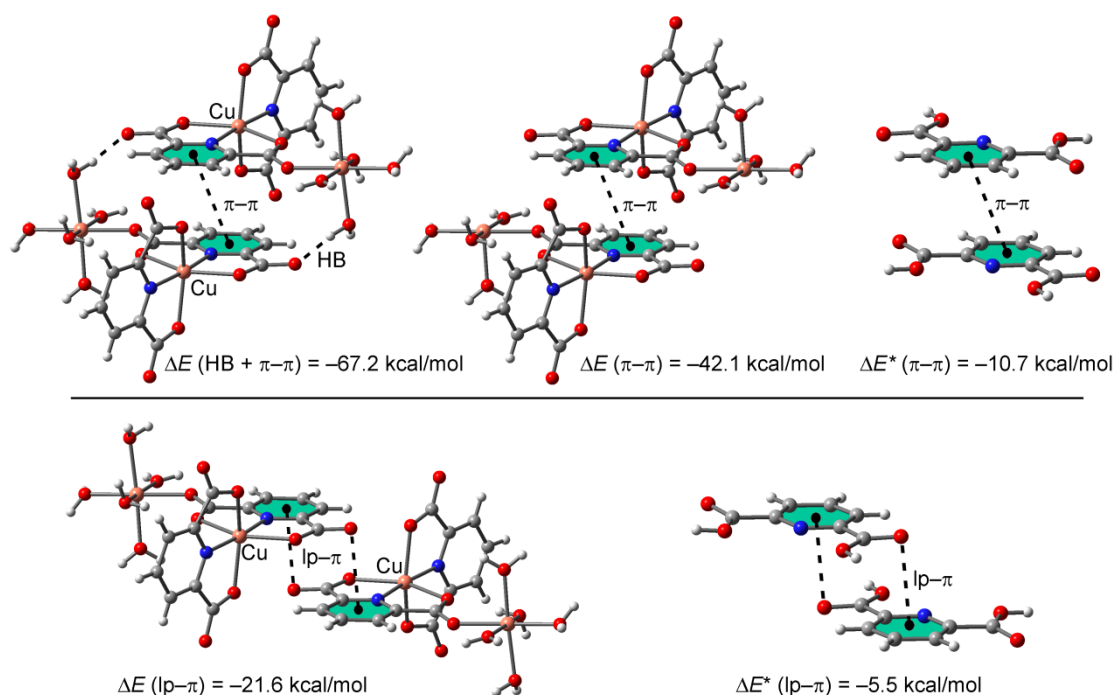


Fig. 16 Theoretical models and interaction energies computed for **3**.

carboxylate group is remarkable. It presents a very short distance ( $< 3\text{\AA}$ ) and, using high level DFT calculations, the interaction has been energetically studied and confirmed by means of the AIM analysis. Furthermore, the formation of an “inverse sandwich” ( $lp-\pi^*-lp$  assembly) in compound **2** is noteworthy. Theoretically, we have demonstrated that such assembly is possible because the  $\pi$ -acidity of the pyrazine ring is enhanced by the coordination of the aromatic nitrogen atoms to the  $\text{Co}^{\text{II}}$  metal ions. Crystal engineering covers in-depth understanding of weak intermolecular interactions that govern crystal packing, thus hypothetically allowing a rational design of solids with tailored physical and chemical properties. The results described above are surely of importance in this regard.

### Acknowledgement

MM and HEH wish to thank to the Ferdowsi University of Mashhad for financial support of this article (Grant No. 19023/3). AB and AF thank DGICYT of Spain (CTQ2011-27512/BQU and CONSOLIDER INGENIO CSD2010-00065, FEDER funds) and the Direcció General de Recerca i Innovació del Govern Balear (project 23/2011, FEDER funds) for funding. The support of NSF-MRI Grant #1228232 for the purchase of the D8 Venture diffractometer is gratefully acknowledged. PB thanks the Gobierno de España MINECO (project CTQ2011-23014), Generalitat de Catalunya DURSI (2009SGR00686) and ICIQ Foundation for funding.

### Notes and references

<sup>a</sup> Department of Chemistry, Ferdowsi University of Mashhad, Mashhad 917751436, Iran, E-mail: mirzaeesh@um.ac.ir

<sup>b</sup> Departament de Química, Universitat de les Illes Balears, Palma de Mallorca (Balears), Spain

<sup>c</sup> Institute of Chemical Research of Catalonia (ICIQ), Avda. Països Catalans 16, 43007 Tarragona, Spain and Catalan Institution for Research and Advanced Studies (ICREA), Passeig Lluís Companys, 23, 08018, Barcelona, Spain.

<sup>d</sup> Department of Chemistry, Tulane University, New Orleans, LA 70118, USA

† CCDC 963267–963273 (for **1–4**) contain the supplementary crystallographic data for this paper.

Electronic Supplementary Information (ESI) available: Some additional figures of the crystal packing of compounds **1–4** and details of the CSD search. See DOI: 10.1039/b000000x/

- 1 G. R. Desiraju, *Crystal Engineering: The Design of Organic Solids*, Ed: Elsevier Science Publishers, B. V.: Amsterdam, The Netherlands, 1989.
- 2 C. B. Aakeröy, A. M. Beatty and B. A. Helfrich, *Angew. Chem. Int. Ed.*, 2001, **40**, 3240.
- 3 A. D. Jana, S. C. Manna, G. M. Rosair, M. G. B. Drew, G. Mostafa and N. R. Chaudhuri, *Cryst. Growth Des.*, 2007, **7**, 1365; N.J. Singh, H.M. Lee, S. B. Suh and K. S. Kim, *Pure Appl. Chem.*, 2007, **79**, 1057; J.Y. Lee, B. H. Hong, W. Y. Kim, S. K. Min, Y. Kim, M. V. Jouravlev, R. Bose, K.S. Kim, I.-C. Hwang, L.J. Kaufman, C. W. Wong, P. Kim and K. S. Kim, *Nature*, 2009, **460**, 498.
- 4 T. S. Thakur and G. R. Desiraju, *Cryst. Growth Des.*, 2008, **8**, 4031.
- 5 S. L. Price, *Acc. Chem. Res.*, 2009, **42**, 117.

- 6 P. J. Kim, J. H. Jeong, M. Jazbinsek, S. B. Choi, I. H. Beak, J. T. Kim, F. Rotermund, H. Yun, Y. S. Lee, P. Günter and O. P. Kwon, *Adv. Funct. Mater* 2012, **22**, 200–209; P. J. Kim, M. Jabinsek, J. H. Jeong, J. T. Kim, Y. S. Lee, Y. M. Jung, S. W. Lee and O. P. Kwon, *CrystEngComm* 2012, **14**, 3633–3637.
- 7 G. A. Jeffrey, *An Introduction to Hydrogen Bonding*, Oxford University Press: Oxford, 1997; G. R. Desiraju and T. Steiner, *The Weak Hydrogen Bond in Structural Chemistry and Biology*, Oxford University Press: Oxford, 1999.
- 8 C. A. Hunter and J. K. M. Sanders, *J. Am. Chem. Soc.*, 1990, **112**, 5525; S. K. Burley and G. A. Petsko, *Science*, 1985, **229**, 23.
- 9 J. C. Ma and D. A. Dougherty, *Chem. Rev.* 1997, **97**, 1303; D. Kim, S. Hu, P. Tarakeshwar, K. S. Kim and J. M. Lisy, *J. Phys. Chem. A*, 2003, **107**, 1228; K. S. Kim, J. Y. Lee, S. J. Lee, T.–K. Ha and D. H. Kim, *J. Am. Chem. Soc.*, 1994, **116**, 7399.
- 10 M. Nishio, M. Hirota and Y. Umezawa, *The C–H/ $\pi$  Interaction: Evidence, Nature and Consequences*, Wiley–VCH, New York, 1998; M. Nishio, *CrystEngComm*, 2004, **6**, 130.
- 11 T. J. Mooibroek and P. Gamez *CrystEngComm*. 2012, **14**, 1027.
- 12 A. Frontera, P. Gamez, M. Mascal, T. J. Mooibroek and J. Reedijk, *Angew. Chem. Int. Ed.* 2011, **50**, 9564–9583; B. L. Schottel, H. T. Chifotides and K.R. Dunbar, *Chem. Soc. Rev.*, 2008, **37**, 68; T.J. Mooibroek, C.A. Black, P. Gamez and J. Reedijk, *Cryst. Growth Des.*, 2008, **8**, 1082; T. J. Mooibroek, S. J. Teat, C. Massera, P. Gamez and J. Reedijk, *Cryst. Growth Des.*, 2006, **6**, 1569; P. Gamez, T. J. Mooibroek, S. J. Teat and J. Reedijk, *Acc. Chem. Res.*, 2007, **40**, 435; M. Mascal, A. Armstrong and M. D. Bartberger, *J. Am. Chem. Soc.*, 2002, **124**, 6274; D. Quiñero, C. Garau, C. Rotger, A. Frontera, P. Ballester, A. Costa and P. M. Deyà, *Angew. Chem. Int. Ed.*, 2002, **41**, 3389; I. Alkorta, I. Rozas and J. Elguero, *J. Am. Chem. Soc.*, 2002, **124**, 8593.
- 13 S. K. Seth, *CrystEngComm*, 2013, **15**, 1772; P. Manna, S. K. Seth, A. Bauza, M. Mitra, S. R. Choudhury, A. Frontera, and S. Mukhopadhyay, *Cryst. Growth Des.*, 2014, **14**, 747.
- 14 K. M. Al–Ahmary, M. Habeeb and E. A. Al–Solmy, *J. Mol. Liquids*, 2011, **158**, 161; G. Gregoire, C. Jouvet, C. Dedonder and A.L. Sobolewski, *J. Chem. Phys.*, 2006, **324**, 398; Y. E. Alexeev, B. I. Kharisov, T. C. Hernandez and A.D. Garnovski, *Coord. Chem. Rev.*, 2010, **254**, 794.
- 15 C. Biswas, M. G. B. Drew, D. Escudero, A. Frontera and A. Ghosh, *Eur. J. Inorg. Chem.*, 2009, 2238; C. Biswas, M. G. B. Drew, M. Estrader and A. Ghosh, *Dalton Trans.*, 2009, 5015; A. Shokrollahi, M. Ghadermazi, F. Manteghi, S. Mehdizadeh, N. Kakaei, M. Shamsipur and Z. Malekhosseini, *J. Iran. Chem. Soc.*, 2011, **8**, 919.
- 16 Y.H. Liu, M. S. Mehata and J.Y. Liu, *J. Phys. Chem.*, 2011, **115**, 19; H. Eshtiagh–Hosseini, H. Aghabozorg, M. Mirzaei, S. A. Beyramabadi, H. Eshghi, A. Morsali, A. Shokrollahi and R. Aghaei, *Spectrochim. Acta Part A: Mol. Biomol. Spectr.*, 2011, **78**, 1392; M. Mirzaei, H. Aghabozorg and H. Eshtiagh–Hosseini, *J. Iran. Chem. Soc.*, 2011, **8**, 580; H. Eshtiagh–Hosseini, M. Mirzaei, S. Zarghami, A. Bauzá, A. Frontera, J. T. Mague, M. Habibi and M. Shamsipur, *CrystEngComm.*, 2014, DOI: 10.1039/C3CE41730A; M. Mirzaei, H. Eshtiagh Hosseini, M. Chahkandi, N. Alfi, A. Shokrollahi, N. Shokrollahi and A. Janiak, *CrystEngComm.*, 2012, **14**, 8468; M. Mirzaei, H. Eshtiagh–Hosseini, S. Zarghami, Z. Karrabi, M. Saeedi and J.T. Mague, *Acta Cryst.*, 2013, **E69**, m128; M. Mirzaei, H. Eshtiagh–Hosseini, Z. Karrabi and B. Notash, *Acta Cryst.*, 2013, **C69**, 1140.
- 17 M. M. Habeeb and R. M. Alghanmi, *J. Chem. Eng. Data.*, 2010, **55**, 930.
- 18 S. Jin, L. Liu, D. Wang and J. Guo, *Journal of Molecular Structure.*, 2011, **59**, 1005.
- 19 H. Eshtiagh–Hosseini, M. Mirzaei, M. Biabani, V. Lippolis, M. Chahkandi and C. Bazzicalupi, *CrystEngComm.*, 2013, **15**, 6752; S. H. Kazemi Riabi, H. Eshtiagh Hosseini, M. Izadyar and M. Mirzaei, *Phys. Chem. Res.*, 2013, **1**, 19; S. H. Kazemi Riabi, H. Eshtiagh–Hosseini and M. Mirzaei, *Comput. Theor. Chem.*, 2013, **69**, 1004; M. Mirzaei, H. Eshtiagh–Hosseini, N. Alfi, H. Aghabozorg, J. Attar Gharamaleki, S. A. Beyramabadi, H. R. Khavasi, A. Salimi, A. Shokrollahi, R. Aghaei and E. Karami, *Struct. Chem.*, 2011, **22**, 1365; M. Mirzaei, V. Lippolis, H. Eshtiagh–Hosseini and M. Mahjoobizadeh, *Acta Cryst.*, 2011, **C68**, 7; H. Aghabozorg, N. Firoozi, L. Roshan, H. Eshtiagh–Hosseini, A. Salimi, M. Mirzaei, M. Ghanbari, M. Shamsipur and M. Ghadermazi, *J. Iran. Chem. Soc.*, 2011, **8**, 992; M. Mirzaei, H. Eshtiagh–Hosseini, V. Lippolis, H. Aghabozorg, D. Kordestani A. Shokrollahi, R. Aghaei and A. J. Blake, *Inorg. Chim. Acta*, 2011, **370**, 141.
- 20 Bruker AXS (2012). *APEX2*, Madison, WI
- 21 Bruker AXS (2012). *SAINT*, Madison, WI
- 22 Bruker AXS (2012). *SADABS*, Madison, WI
- 23 Sheldrick, G. M. (2008). *SHELXS* and *SHELXL*. *Acta Cryst.* **A64**, 112.
- 24 M. C. Burla, R. Caliandro, M. Camalli, B. Carrozzini, G.L. Cascarano, C. Giacovazzo, M. Mallamo, A. Mazzone, G. Polidori and R. Spagna, *J. Appl. Cryst.*, 2012, **45**, 357–361.
- 25 R. Ahlrichs, M. Bär, M. Haser, H. Horn and C. Kölmel, *Chem. Phys. Lett.*, 1989, **162**, 165–169.
- 26 S. F. Boys and F. Bernardi, *Mol. Phys.*, 1970, **19**, 553.
- 27 R. F. W. Bader. *Chem. Rev.*, 1991, **91**, 893–928.
- 28 AIMAll (Version 13.11.04), T. A. Keith, TK Gristmill Software, Overland Park KS, USA, 2013.
- 29 M. Solimannejad, V. Ramezani, C. Trujillo, I. Alkorta, G. Sanchez–Sanz and J. Elguero, *J. Phys. Chem. A.*, 2012, **116**, 5199–5206.
- 30 Y. Lu, Y. Liu, H. Li, X. Zhu, H. Liu and W. Zhu, *J. Phys. Chem. A* 2012, **116**, 2591–2597.
- 31 U. Koch and P. L. A. Popelier, *J. Phys. Chem.*, 1995, **99**, 9747–9754